Soot accumulation and combustion in porous media

Kazuhiro Yamamoto[*1] **and Fumihiro Ochi** [1]

Although diesel engines have an advantage of low fuel consumption compared with gasoline engines, several problems must be solved. One of the major concerns is that diesel exhaust gas has more particulate matters (PM) including soot, which are suspected to be linked to human carcinogen. As one of the key technologies, a diesel particulate filter (DPF) has been developed to reduce PM in the after-treatment of exhaust gas. In this study, we simulate soot accumulation and combustion in simplified porous media by the Lattice Boltzmann method. Results show that the flow pattern is largely changed when the soot is accumulated. In combustion simulation, the reaction is well simulated to observe the reduction of accumulated soot with temperature increase near the porous wall. Our approach can be used to capture the dynamics of soot behaviors in porous media flow for better design of DPF.

Nagoya University, Furo-cho, Chikusa-ku, Nagoya, Aichi 464-8603 JAPAN
Tel&Fax: +81-52-789-4471 E-mail: kazuhiro@mech.nagoya-u.ac.jp
Key words: Soot, Diesel particulate filter, Porous media, Combustion, Lattice Boltzman method

INTRODUCTION

Recently, the share of a diesel car in the world is gradually increased, because diesel engines have an advantage of low fuel consumption in comparison with gasoline engines. However, several problems must be solved. One of the major concerns is that diesel exhaust gas has more particulate matters (PM) including soot, which are suspected to be linked to human carcinogen. For this reason, more strict exhaust emissions standards such as Euro V in 2008 will be setting in many countries. In Japan, the Tokyo municipal government has begun to regulate diesel-powered commercial vehicles that fail to meet their new emission standards.

As one of the key technologies, a diesel particulate filter (DPF) has been developed to reduce PM in the after-treatment of exhaust gas, which can be applied to satisfy more strict regulations for diesel emissions, coupled with improvements of combustion conditions. Some products have been already introduced at the Frankfurt Motor Show in 2003. In simple explanation of DPF, it traps the particles when exhaust gas passes its porous structure. Since the filter wall would readily be plugged with particles in a short time, the accumulated particles must be removed. Usually, the filter is heated to burn particles in combustion. It is called filter regeneration process. However, it is expected that the outer heating with the particle burning may destroy the porous structure. Then, the thermal durable filter is plausible to maintain the low level of emissions in the long term.[1] So far, the filter has been developed mainly by experiments, and there may not be enough information to observe and understand the phenomena in DPF. For better design of DPF with efficiency and durability, it is necessary to conduct simulation with combustion in porous filter. In conventional computational code, it is very challenging to deal with this process, because we need to consider the complex geometry with chemical reaction.

In the Lattice Boltzmann method (LBM), the treatment of boundary conditions is simple and easy, and it is appropriate to calculate porous media flow.[2-7] The particle deposition in filter material has been also simulated by LBM.[8] Recently, we have simulated the combustion flow in three-dimensional porous structure by LBM.[9] To consider the flow in a real porous media, three-dimensional computer tomography technique (3D CT [10,11]) has been applied to obtain inner structure of a Ni-Cr metal. The flow with combustion reaction has been well simulated to

discuss the local heat and mass transfer for the regeneration process of DPF.

In our previous study, it is assumed that the soot concentration is initially constant at the porous wall surface. However, it is expected that the particles including soot are inhomogeneously attached to the wall in DPF. To consider the real situation, we need to simulate the particle accumulation in porous media. Here, we develop numerical scheme for simulating soot decomposition in fluids. Then, we can investigate the filter regeneration process under inhomogeneous combustion reaction.

NUMERICAL METHOD

The numerical scheme for combustion simulation by LBM is explained in our previous paper.[12] Here, the incompressible 2D square Lattice BGK model (d2q9) is used. To consider the variable density, we adopt the low Mach number approximation.[13] Formula of numerical scheme for flow, temperature, and concentration fields are briefly explained here.

The 9-bit lattice BGK model evolves on the two-dimensional square lattice space with the following 9 discrete velocities[14]:

$$\boldsymbol{e}_\alpha = \begin{cases} (0,\ 0) & (\alpha = 0) \\ (\cos[(\alpha-1)\pi/2],\ \sin[(\alpha-1)\pi/2])\cdot c & (\alpha = 1\text{-}4) \\ (\cos[(\alpha-5)\pi/2+\pi/4],\ \sin[(\alpha-5)\pi/2+\pi/4])\sqrt{2}\cdot c & (\alpha = 5\text{-}8) \end{cases} \quad (1)$$

where $c = \delta_x/\delta_t$, and δ_x and δ_t are the lattice constant and the time step, respectively. The evolution equation for fluid is

$$p_\alpha(\boldsymbol{x}+\boldsymbol{e}_\alpha\delta_t,\ t+\delta_t) - p_\alpha(\boldsymbol{x},\ t) = -\frac{1}{\tau}[p_\alpha(\boldsymbol{x},\ t) - p_\alpha^{eq}(\boldsymbol{x},\ t)] \quad (2)$$

$$p_\alpha^{eq} = w_\alpha\left\{p + p_0\left[3\frac{(\boldsymbol{e}_\alpha\cdot\boldsymbol{u})}{c^2} + \frac{9}{2}\frac{(\boldsymbol{e}_\alpha\cdot\boldsymbol{u})^2}{c^4} - \frac{3}{2}\frac{\boldsymbol{u}^2}{c^2}\right]\right\} \quad (3)$$

where $w_0 = 4/9$, $w_\alpha = 1/9$ (α = 1-4), $w_\alpha = 1/36$ (α = 5-8). The sound speed, c_s, is $c/\sqrt{3}$, and $p_0=\rho_0 c_s^2$. The pressure, p, and velocity, $\boldsymbol{u}=(u_x, u_y)$, are calculated by

$$p = \sum_\alpha p_\alpha \quad (4)$$

$$p_0\boldsymbol{u} = \sum_\alpha \boldsymbol{e}_\alpha p_\alpha \quad (5)$$

Through the Chapman-Enskog procedure, the incompressible Navier-Stokes equations are derived from these equations.[15] The kinetic viscosity is

$$\nu = \frac{2\tau-1}{6}\frac{\delta_x^2}{\delta_t} \quad (6)$$

Formula for temperature and concentration fields are as follows:

$$F_{s,\alpha}(\boldsymbol{x}+\boldsymbol{e}_\alpha\delta_t,\ t+\delta_t) - F_{s,\alpha}(\boldsymbol{x},\ t) = -\frac{1}{\tau_s}[F_{s,\alpha}(\boldsymbol{x},\ t) - F_{s,\alpha}^{eq}(\boldsymbol{x},\ t)] + w_\alpha Q_s \quad (7)$$

$$F_{s,\alpha}^{eq} = w_\alpha s\left\{1 + 3\frac{(\boldsymbol{e}_\alpha\cdot\boldsymbol{u})}{c^2} + \frac{9}{2}\frac{(\boldsymbol{e}_\alpha\cdot\boldsymbol{u})^2}{c^4} - \frac{3}{2}\frac{\boldsymbol{u}^2}{c^2}\right\} \quad (8)$$

$s = T,\ Y_i$ (i = C, O_2 , CO_2, N_2).

The temperature, T, and mass fraction of species i, Y_i, are obtained in terms of the distribution function by

$$T = \sum_\alpha F_{T,\alpha} \quad (9)$$

$$Y_i = \sum_\alpha F_{Yi,\alpha} \quad (10)$$

The source term due to chemical reaction, Q_s, is given by the similarity in non-dimensional equations of temperature and concentration fields. For soot oxidation, the over-all reaction by Lee et al. is adopted.[16] More information on soot oxidation is found in the review article by Stanmore et al.[17] For simplicity, any catalytic effect is not considered.

To simplify the porous media, we consider the duct flow with obstacles. Figure 1 shows the calculation domain and coordinate. The size is 5 cm × 1 cm, and the inflow velocity, U_{in}, is 20 cm/s. The total number of grids is 201×41, with grid size of

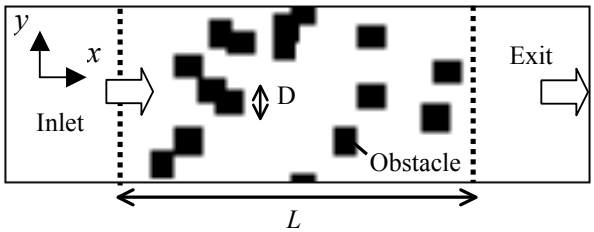

Fig. 1 Calculation domain and coordinate.

0.25 mm. To change the flow characteristics such as porosity and tortuosity, the different number and size of obstacle are used, which are placed randomly in the center part between two dotted lines in this figure. Its size is 100-grid length (L). In Ref. 9, it is confirmed that the flow characteristics in the duct flow with obstacles obey the so-called Ergun equation, the empirical equation in porous media flow.[18] In the calculation, all equations are non-dimensionalized, and the real properties such as temperature and concentration are taken into account based on similarity.

As for the boundary conditions, the inflow boundary is adopted at the inlet.[19] The temperature and mass fractions are those of the air at room temperature. At the sidewall, the slip boundary conditions are adopted, considering the symmetry.[12] At the outlet, the pressure is constant, and the gradient of scalar such as temperature is set to be zero. On the surface of obstacles, the bounce-back rule for non-slip boundary condition is adopted. The particle deposition model by Chopard et al. is used.[20] The soot concentration is monitored around the obstacles. Due to the soot accumulation, its concentration becomes unity. When this limit is reached, the solid site is piling up. The accumulated soot region is treated as non-slip wall. Thus, this solidification process implies a dynamically change of boundary condition for fluid.

RESULTS AND DISCUSSION

First of all, before we simulate the flow field with soot, an effect of porosity is examined. Three simulations are conducted. For all cases, the number of obstacles is 55 in the calculation domain, but its size is of D = 2, 3, 4 in lattice space, which are 0.5, 0.75, 1.0 mm in real scale. The resultant porosity, e, are 0.95, 0.89, and 0.81, respectively. Figure 2 shows the distribution of non-dimensional velocity in the x-direction, u_x/U_{in}. The flow is largely fluctuated in the area with obstacles, even when the flow is uniform at the inlet. The velocity is increased in the narrow path between obstacles. This acceleration is locally different, since the obstacle is randomly placed. As a whole, the flow is smooth when the obstacle is small. The maximum velocity is larger as the porosity is smaller. In the case of D = 4, the negative velocity is observed, which means that the recirculation flow exists. When the soot is accumulated on the obstacle surface, the solid sites are similarly enlarged. Then, the flow pattern will be changed with soot deposition.

Next, the pressure distribution is examined for above three cases, which is an important parameter

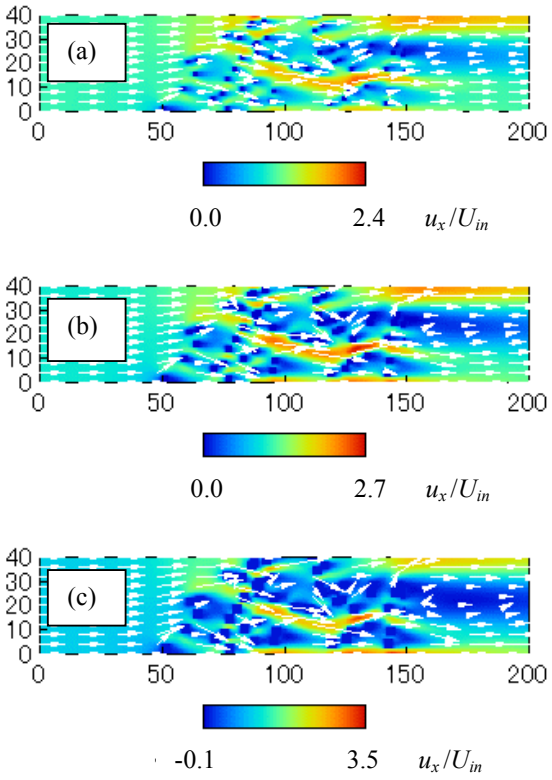

Fig. 2 Flow field with obstacles, (a) D = 2, e = 0.95, (b) D = 3, e = 0.89, and (c) D = 4, e = 0.81.

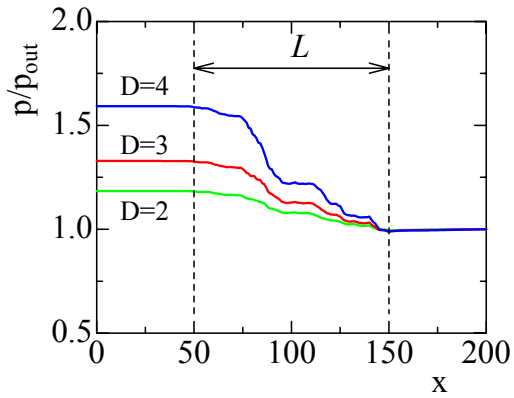

Fig. 3 Pressure distribution in the flow direction for D = 2; e = 0.8, 0.9, and 0.95.

in porous media flow.[18] Figure 3 shows the pressure distribution, which is the mean value in cross section, normalized by the constant pressure at the outlet. In the area with obstacles, the pressure starts to decrease almost linearly. After passing this region, the pressure is almost constant. To compare three cases, it is found that, when the porosity is smaller, the pressure at the inlet is larger. This is explained by the fact that the surface of the obstacle is wider with larger obstacle, causing the larger effect of shear forces.

Then, we simulate the flow with soot in this duct flow. Initially, the obstacle of $D = 2$ are placed. The porosity is 0.98. Figure 4 shows time evolution of soot accumulation. The mass fraction of soot at the inlet, $Y_{C,in}$, is 0.005. These profiles are obtained at t = 0.37, 0.50, and 0.63. After the soot is attached to the obstacles, the flow pattern is changed. The soot is preferlably accumulated upstream. We can not calculate the flow when the channel is completely plugged with soot. Figure 5 shows the pressure distribution at t = 0.3 s. The initial distribution without soot is also shown. It is found that the pressure at the inlet is increased when the soot is accumulated. The similar pressure change is observed when the deposited layer is developed in the gas-particle flow.[8]

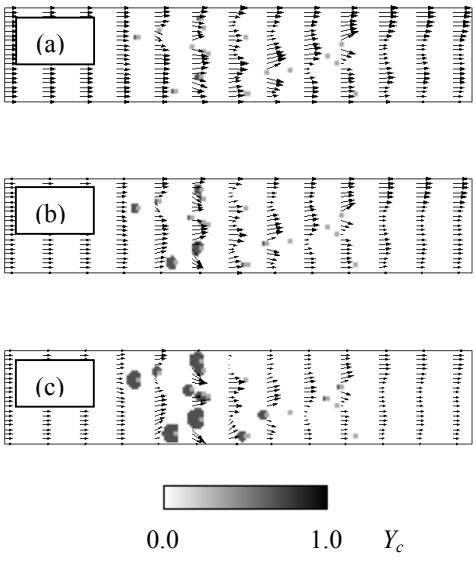

Fig. 4 Accumulation of soot with velocity vector; (a) t = 0.37s, (b) t = 0.5 s, and (c) t = 0.63 s.

To see the effect of inlet soot concentration, the averaged accumulated soot is calculated. It is the averaged mass fraction of soot in the calculation domain. We simulate three cases with $Y_{C,in}$ = 0.01, 0.0075, 0.005. Results are shown in Fig. 6. Gradually, the mass of deposited soot starts to increase. Then, its increase rate becomes very large, because surface area where the soot can be attached is expanded. When the soot concentration is higher at the inlet, the accumulated soot is expectedly increased.

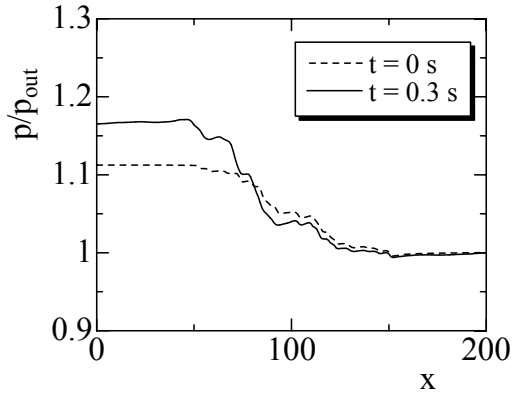

Fig. 5 Pressure distributions with soot accumulation.

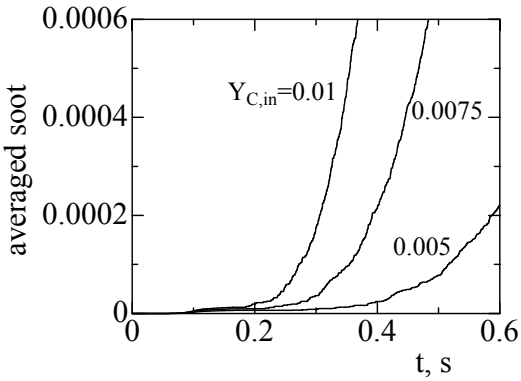

Fig. 6 Averaged accumulated soot with different inlet condition.

Finally, the combustion flow is simulated. We choose the soot distributions in Fig. 4c as the initial soot profile. The inflow is air and the mass fraction of oxygen is 0.233. When the solid site of both obstacle and deposited soot is heated, the soot is burned to react with oxygen. The soot distributions at different time steps are shown in Fig. 7. Time, t, is counted after we set the temperature at solid site to be 1200 K, and these are profiles at t = 0, 1.9, and 5.0 s. As seen in this figure, the soot is gradually consumed by combustion reaction.

Figure 8 shows the distributions of temperature, T, mass fraction of oxygen and soot, Y_{O2} and Y_C, and reaction rate, W_c. The temperature and reaction rate are non-dimensionalized by room temperature and the maximum reaction rate, respectively. The real time is 0.63 s after heating. Both oxygen and soot concentration around the obstacles is decreased by the combustion reaction. Then, the maximum temperature is higher than the heated temperature. It is interesting to note that the degree of soot consumption rate is locally different, simply because the oxygen transport in the flow with complex geometry is different by the convection.

In addition, we change the oxygen concentration in inflow. The oxygen concentration can be an important parameter in engine operation, because it is easy to control the oxygen concentration by using the exhaust gas recirculation (EGR)[21], in order to prevent an abrupt temperature rise from damaging the local structure of DPF. Here, nitrogen is added in the air. We set the oxygen concentration (mass fraction) to be 0.233 (air) and 0.1. As seen in Fig. 8d, the reaction rate is locally changed. To make clear the effect of oxygen concentration, the reaction rate is averaged in the surface of deposited soot. Results are shown in Fig. 9. In the case of the lower oxygen concentration, the mean reaction rate is decreased. That is, the reaction of soot can be reduced to avoid the large heat release rate, compared with non-dilution case.

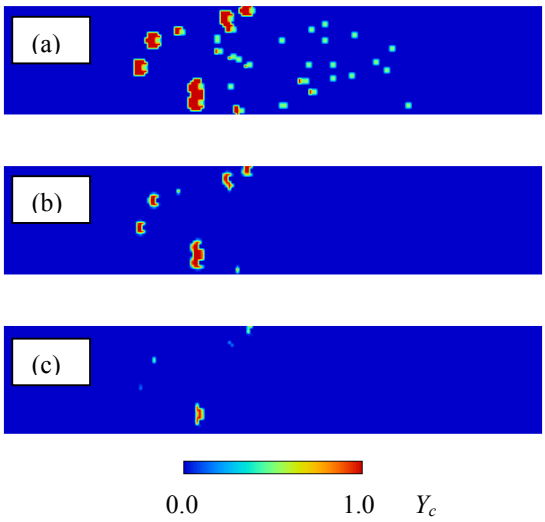

Fig. 7 Soot distributions at (a) t = 0 s, (b) t = 1.9 s, and (c) t = 5.0 s.

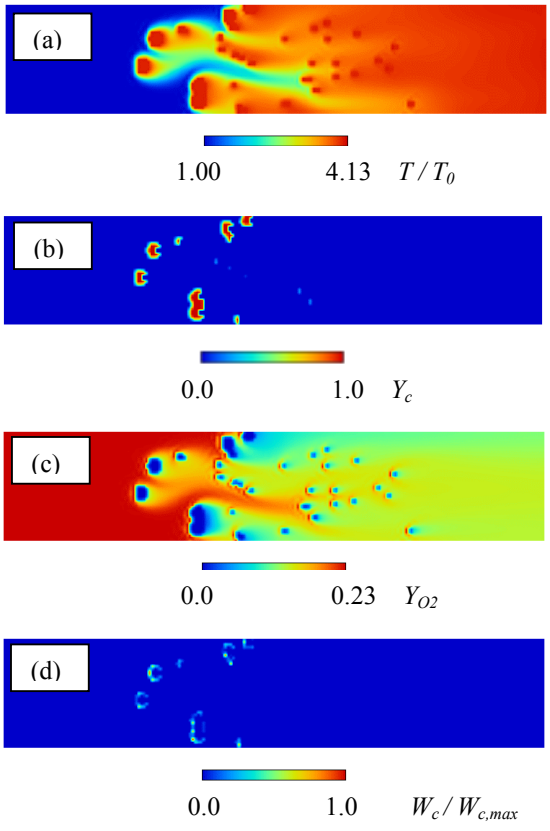

Fig. 8 Distributions of (a) temperature, (b) oxygen, (c) soot, and (d) reaction rate at t = 0.63 s.

CONCLUSIONS

We have simulated the soot accumulation and combustion in porous media. The particle deposition model by Chopard et al. is adopted. It is found that the flow pattern is largely changed when the soot is accumulated. When we change the soot concentration at the inlet, the degree of soot accumulation is apparently different. Then, combustion simulation is conducted to burn the deposited soot. As the soot is heated, combustion occurs near the obstacle surface

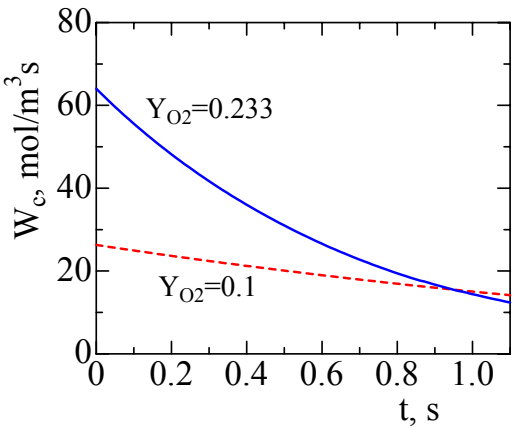

Fig. 9 Mean reaction rate of soot as a function of time, with oxygen mass fraction of 0.1 and 0.233 in inlet flow.

to decrease the soot concentration with temperature rise. As the oxygen concentration is lower, the mean reaction rate is reduced. Our approach can be used to capture the dynamics of soot behaviors in porous media flow for the better design of DPF.

REFERENCES

1. R. A. Searles, D. Bosteels, C. H. Such, A. J., J. D. Andersson, and C. A. Jemma, 2002, Investigation of the Feasibility of Achieving Euro V Heavy-Duty Emissions Limits with Advanced Emission Control Systems, F02E310, *FISITA 2002 World Congress,* 1-17.
2. G. McNamara, and G. Zanetti, 1988, Use of the Boltzmann Equation to Simulate Lattice-Gas Automata, *Phys*. *Re*6. *Lett*., **61**, 2332–2335.
3. S. Succi, E. Foti, and F. Higuera, 1989, Three-Dimensional Flows in Complex Geometries with the Lattice Boltzmann Method, *Europhys*. *Lett*., **10**, 433–438.
4. A. Cancelliere, C. Chang, E. Foti, D. H. Rothman, and S. Succi, 1990, The Permeability of a Random Medium: Comparison of Simulation with Theory *Phys*. *Fluids A*, **2**, 2085–2088.
5. Y. H. Qian, D. d'Humie`res, and P. Lallemand, 1992, Lattice BGK Models for Navier-Stokes Equation, *Europhys*. *Lett*., **17**, 479–484.
6. T. Inamuro, M. Yoshino, and F. Ogino, 1999, Lattice Boltzmann Simulation of Flows in a Three-dimensional Porous Structure, *Int. J. Numerical Methods in Fluids* **29**, 737-748.
7. J. Bernsdorf, G. Brenner, and F. Durst, 2000, Numerical Analysis of the Pressure Drop in Porous Media Flow with Lattice Boltzmann (BGK) Automata, *Computer Physics Communications* **129**, 247-255.
8. O. Filippova, and D. Hänel, 1997, Lattice-Boltzmann Simulation of Gas-Particle Flow in Filters, *Computers & Fluids* **26**, 697-712.
9. K. Yamamoto, N. Takada, and M. Misawa, 2005, Combustion Simulation with Lattice Boltzmann Method in a 3D Porous Structure, *Proc. Comb. Inst.* **30**, 1505-1515.
10. A. H. Benouali, L. Froyen, M. Wevers, 2000, *X-ray Tomography in Material Science*, 129-153.
11. M. Misawa, N. Takada, I. Tiseanu, R. Hirashima, and K. Koizumi, 2002, Development of Oblique View Cone Beam Tomography System, *The Papers of Technical Meeting on Nuclear Energy, IEE Japan*, NE-02-14, 17-22.
12. K. Yamamoto, X, He, and G. D. Doolen, 2002, Simulation of Combustion Field with Lattice Boltzmann Method, *J. Statistical Physics*, Vol. 107, Nos.1/2, 367-383.
13. O. Filippova, and D. Hänel, 1998, Lattice-BGK Model for Low Mach Number Combustion, *Int. J. Modern Physics C* **9**, 1439-1445.
14. X. He, and L. –S. Luo, Lattice Boltzmann Model for the incompressible Navier-Stokes Equation, *J. Statistical Physics*, Vol. 88, Nos.3/4, 927-944.
15. S. Chen, and G. D. Doolen, 1998, Lattice Boltzmann Method for Fluid Flows, *Annual Reviews of Fluid Mech.* **30**, 329-364.
16. K. B. Lee, M. W. Thring, and J. M. Beer, 1962, On the Rate of Combustion of Soot in a Laminar Soot Flame, *Comb. Flame* 6, 137-145.
17. B. R. Stanmore, J. F. Brilhac, and P. Gilot, 2001, The Oxidation of Soot: A Review of Experiments, Mechanisms and Models, *Carbon* **39**, 2247-2268.
18. R. B. Bird, W. E. Stewart, and E. N. Lightfoot, 1960, *Transport Phenomena*, Wiley, New York.
19. Q. Zou and X. He, 1997, On Pressure and Velocity Boundary Conditions for the Lattice Boltzmann BGK Model, *Phys. Fluids 9 (6)*, 1591-1598.
20. B. Chopard, A. Masselot, and A. Dupuis, 2000, A Lattice Gas Model for Erosion and Particle Transport in a Fluid, *Computer Physics Communications* **129**, 167-176.
21. K. N. Pattas, A. M. Stamataelos, K. N. Kougianos, G. C. Koltsakis, and P. K. Pistikopoulos, 1996, Trap Protection by Limiting A/F Ratio during Regeneration, *SAE Paper* No. 950366.